THE EFFECTS OF SURFACE CONDITIONS ON BOILING CHARACTERISTICS

J. J. Lorenz
B. B. Mikic
W. M. Rohsenow

December, 1972

Report No. DSR 73413-79
Contract No. DAHC04-71-C-0040

Department of Mechanical Engineering
Engineering Projects Laboratory
Massachusetts Institute of Technology

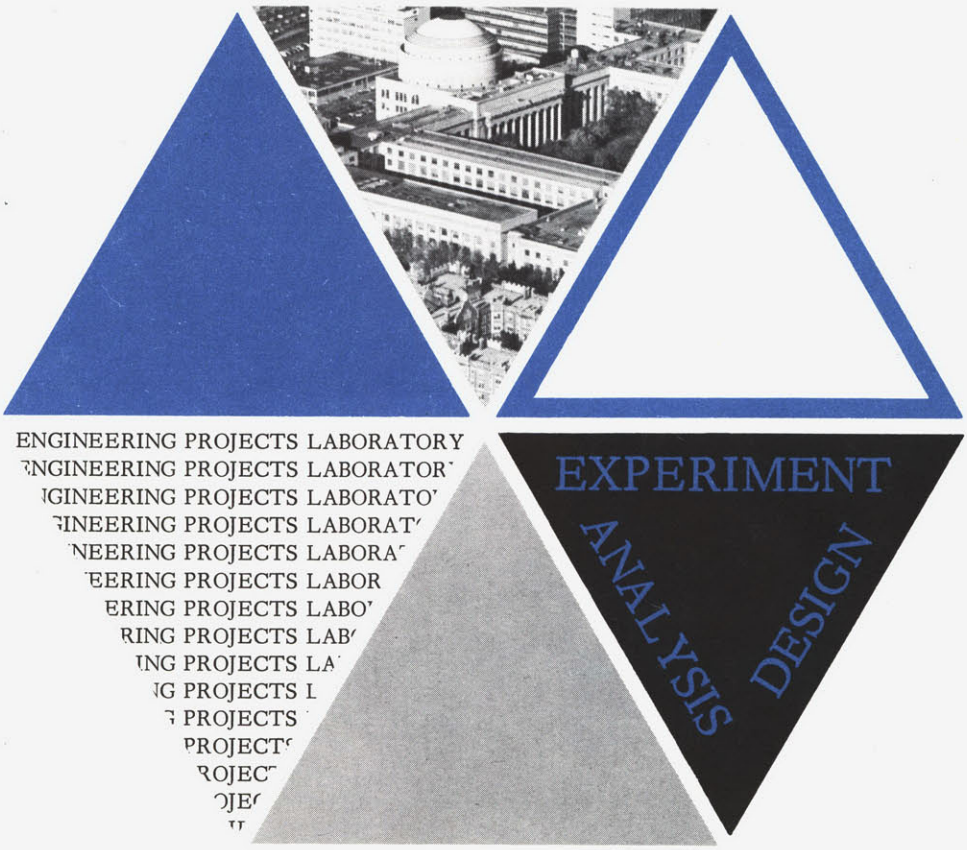

THE EFFECTS OF SURFACE CONDITIONS ON BOILING CHARACTERISTICS

J. J. Lorenz, B. B. Mikic and W. M. Rohsenow

Massachusetts Institute of Technology
Cambridge, Massachusetts 02139

ABSTRACT

A unified model relating surface variables to the nucleate pool boiling characteristics was developed. A simple vapor trapping mechanism was postulated and a geometrical model constructed for idealized conical cavities relating the effective radius for nucleation to cavity radius, cone angle and contact angle. This model for individual cavities was extended to the entire surface providing an expression for the cumulative site density in terms of geometrical parameters. A gas diffusion technique was developed to measure the effective radius for natural cavities and was used successfully to verify the nucleation criteria $\Delta T = 2\sigma T_s v_{fg}/h_{fg}\rho$. A transient heat conduction model was experimentally verified for water and organics at atmospheric pressure and was incorporated into a unified expression showing explicitly the role of surface geometry and contact angle.

ACKNOWLEDGEMENT

The authors are grateful to the U. S. Army Research Office for financial support of this work.

TABLE OF CONTENTS

NOMENCLATURE

A	Surface Area
C	Specific heat and dissolved gas concentration
D_b	bubble departure diameter
f	frequency of bubbles
$f(\theta,\phi)$	dimensionless function, Equation (5)
h	heat transfer coefficient
h_{fg}	latent heat of vaporization
k	thermal conductivity
n/A	number of sites/unit area
P	Pressure
q/A	heat flux
R	cavity radius
T_s	saturation temperature corresponding to system pressure
v_{fg}	specific volume change of evaporation
ΔT	$T_w - T_s$
ρ	radius of curvature of gas-liquid interface
θ	contact angle
ϕ	cone angle
σ	surface tension

SUBSCRIPTS

a	air
b	boiling
ℓ	liquid
O_2	oxygen
s	saturation condition

FIGURE CAPTIONS

INTRODUCTION

This work is primarily concerned with further studies of surface effects on heat transfer in boiling, beyond those in References [1] through [5]. In particular, the behavior of individual cavities in boiling with different liquids was investigated by boiling experiments.

From the nucleation criteria for individual cavities and the cumulative distribution of mouth cavity radii, the number of active sites was related to fluid properties (including the fluid contact angle) and the surface properties, which then was incorporated into an overall heat transfer correlation.

HEAT FLUX MODEL

For conditions under which microlayer evaporation is insignificant, i. e., relatively high system pressure, low wall superheat or subcooled bulk temperature [6], Mikic and Rohsenow [3] developed the following transient conduction model for heat flux in the isolated bubble region of the boiling curve:

$$q/A = (q/A)_b + (q/A)_{NC} = 2\sqrt{\pi}\,\sqrt{(k\rho c)_\ell}\sqrt{f}\,D_b^{\,2}\Delta T\,\frac{n}{A} + (1 - \frac{n}{A}\pi D_b^{\,2})h_{NC}\Delta T. \qquad (1)$$

In this equation $(q/A)_b$ and $(q/A)_{NC}$ are the boiling and natural convection components of the heat flux, respectively, and h_{NC} is the natural convection heat transfer coefficient.

For the boiling component only, one can write:

$$(q/A)_b^{\,*} \equiv \frac{(q/A)_b}{2\sqrt{\pi}\,\sqrt{(k\rho c)_\ell}\,\sqrt{f}\,D_b^{\,2}\Delta T} = \frac{n}{A}. \qquad (2)$$

This equation shows that $h_b = (q/A)_b/\Delta T \sim n/A$.

NUCLEATION

Griffith and Wallis [7] verified the following nucleation criterion for incipient nucleation from artificial cavities in a uniformly superheated system:

$$\Delta T = \frac{2\sigma T_s v_{fg}}{h_{fg}\rho}. \qquad (3)$$

Some investigators [11-15] propose modifications of this model to account for a temperature gradient near the surface.

For small natural cavities, at the flux level in the isolated bubble region, Equation (3) should be applicable.

EFFECTIVE RADIUS OF NUCLEATION

The superheat required for a cavity to nucleate, Equation (3), is determined by the value of ρ, which could be considered as an effective radius of nucleation. It is clearly related to the cavity radius, but need not be necessarily identical with it. Figure 1 shows a conical cavity, together with its $1/\rho$ versus vapor volume curve. For a given liquid and a given cavity, ρ could be larger than, equal to, or smaller than R, depending on the vapor volume. If the initial trapped volume is such as to yield $\rho < R$, it is clear from Equation (3) and Figure 1b that this initial ρ determines the required superheat for the cavity activation. On the other hand, if $\rho \geq R$, then the cavity radius R determines the required superheat. The initial value of ρ will depend on the vapor trapping mechanism in the cavity.

Bankoff [16] first described the relationship between contact angle and cone angle which determines whether or not vapor will be trapped.

In wedge-shaped grooves for which $\theta > \phi$ where θ is the contact angle and ϕ is the wedge angle, vapor will not be completely displaced by the advancing liquid front and trapping occurs. If $\theta < \phi$ the vapor will be completely displaced by liquid and the cavity deactivated.

For a conical cavity of radius R and cone angle θ,[1] a similar mechanism could be adopted. Due to a slight asymmetry in the bubble departure, liquid with contact angle θ will advance into the cavity from a favored direction, as shown in Figure 2a. The shape of the liquid surface is assumed nominally flat as the front penetrates into the cavity. Trapping is completed when the liquid surface intersects the opposite edge of the cavity at point A of Figure 2a. A flat liquid surface is certainly an idealization. Also, hydrodynamic effects should be considered in a model that would more accurately describe the liquid surface shape.

If it is assumed that the vapor volume, v_1, trapped in Figure 2a equals the readjusted vapor volume, v_2, in Figure 2b, the magnitude of ρ and hence ρ/R can be determined solely from geometry for any θ and ϕ [17]. Figure 3 gives the results.

Consistent with the model, Figure 3 shows that for $\theta \leq \phi$ no vapor is trapped in the cavity. At any given cone angle ϕ there is a maximum value of contact angle θ above which the effective radius of nucleation would be identical with the cavity radius.

DENSITY OF ACTIVE SITES

It is assumed, as in Reference [3], that the cumulative distribution

---

[1] Natural cavities are not truly conical but only tapered toward the cavity root as observed from microscopic studies. The conical assumption is considered, however, a reasonable approximation.

of mouth radii with cavity radius larger than R is given as:

$$n/A = (R_s/R)^m \tag{4}$$

where m and R_s depend on the surface geometry. Assuming furthermore that a single equivalent cone angle, Φ, can be specified for all the cavities, one can state that

$$\rho/R = f(\theta,\Phi). \tag{5}$$

Combining Equations (4) and (5), the cumulative distribution is:

$$n/A = \left[\frac{R_s \cdot f(\theta,\Phi)}{\rho}\right]^m . \tag{6}$$

For a given surfiace, i. e. given R_s, Φ, and m, Equation (6) together with Figure 3, which gives a value for $f(\theta,\Phi)$, shows how the contact angle affects the cumulative site density. For $\Phi = 5°$, $R_s = 2 \times 10^{-4}$, Figure 4 gives n/A vs. ρ for various values of contact angle θ. Again it can be seen that for this case all the liquids with contact angle greater than 30° have common site distributions; the value of $f(\theta,\Phi)$ for this case is unity. For contact angles less than 30°, $f(\theta,\Phi) < 1$, and the cumulative number of active sites will decrease with decreasing contact angle.

Cumulative site density can be related to the wall superheat by substituting the expression for ρ obtained from Equation (3) into Equation (6) with the following result:

$$n/A = \left[\frac{R_s \cdot f(\theta,\Phi) h_{fg} \Delta T}{2\sigma T_s v_{fg}}\right]^m . \tag{7}$$

HEAT TRANSFER BOILING CORRELATION

It is evident from Equations (7) and (2) that contact angle, in addition to other fluid and surface properties, will affect the boiling heat transfer. This dependence can be explicitly written by combining Equations (7) and (2) as follows:

$$(q/A)_b = \frac{\sqrt{\pi}\,[R_s \cdot f(\theta,\Phi)]^m}{2^{m-1}} (k\rho c)_\ell^{1/2} \left(\frac{h_{fg}}{v_{fg} T_s \sigma}\right)^m \sqrt{f}\, D_b^{\,2} \Delta T^{m+1}. \qquad (8)$$

The expressions for f and D_b, which are needed for evaluation of $(q/A)_b$, can be taken from one of the available correlations (e. g., [18,19]) or more reliably, when possible, taken from reported experimental investigations for corresponding conditions (e. g. [20]).

The conclusions based on the modeling and the analysis presented above are:

(i) Boiling component of the heat flux is directly proportional to n/A (Equation (2)).

(ii) In general, a given cavity will have different effective radii of nucleation for different liquids (Figure 3).

(iii) The cumulative active cavity distribution of a given surface is different for different fluids (Equation (6)), and as a consequence the boiling curve will accordingly be affected (Equation (8)).

EXPERIMENTAL APPARATUS AND PROCEDURE

The experimental equipment necessary for this study consisted of a boiling and gas diffusion apparatus. The boiling apparatus was used to obtain q/A vs. ΔT curves and cumulative nucleation site distributions and to study nucleation from individual sites. The effective radius for natural cavities was determined by the gas diffusion experiments.

Boiling Apparatus and Procedure

Boiling occurred from the end of a 1 in. diameter copper cylinder mounted almost flush with the base of the teflon-coated brass enclosure. Heat was supplied to the straight conductor section by a copper heat section containing a high density cartridge heater. Visual observation of the boiling process was possible through pyrex windows on the front and back of the enclosure. Four thermocouples along the axis of the straight section permitted determination of wall superheat and heat flux while the bulk temperature was measured with a thermocouple placed about 1" above the boiling surface. Data was taken traversing the boiling curve from high to low heat flux. Incrementally the heat flux was lowered and the system allowed to reach equilibrium at which points the thermocouple readings were recorded. When the isolated bubble region was encountered, the number-of-sites/in^2 was determined by visual counting. The test was terminated after a couple of data points were obtained in the natural convection region.

The detailed description of the apparatus and procedures are given in Reference [17].

GAS DIFFUSION EXPERIMENT

Using gas diffusion experiments to study nucleate boiling is not an entirely new idea. Westwater and Buel [21] studied growth of CO_2 bubbles in supersaturated water, looking at the influence of contact angle. By the analogy between heat and mass transfer, certain generalizations can be made regarding boiling systems. One of the most novel uses of a gas diffusion experiment was devised by Brown [22] who claimed it was possible to measure the cumulative nucleation site density for a fluid surface combination with a device called the "Bubble Meter."

Equilibrium Radius

For thermodynamic equilibrium of an air-liquid system across a spherical interface with radius of curvature ρ, the following relation must be satisfied:

$$\rho = \frac{2\sigma}{P_a + P_v - P_\ell} \tag{9}$$

where P_a and P_v are the partial pressures of air and water in the gas phase, and P_ℓ is the pressure of the liquid. In addition, it can be shown [23] that P_v is nearly the saturation pressure corresponding to the system temperature and that the partial pressure of air in gas phase can be related to the concentration of the dissolved air in the liquid phase, C_a, in terms of Henry's constant, m, as

$$P_a = m\, C_a. \tag{10}$$

Apparatus and Procedure

Figure 5 shows the apparatus. The high pressure tank contains deionized water, saturated with dissolved air at the corresponding tank pressure. The water from the tank is allowed to flow into the open tray containing the test surface. With respect to the new condition in the tray (at atmospheric pressure) the liquid is supersaturated and bubble growth is possible. An electric stirrer placed near the test surface insures that no significant concentration gradients develop. An equilibrium bulk concentration will be established among the dissolved gas being supplied at the inlet, that lost at the drain and free surface, and that consumed in bubble growth within the system. By varying the inlet flow rate the concentration can be regulated. An oxygen probe (described in Reference [17]) placed near the test surface continuously monitors this concentration.

If the concentration is sufficiently high, a large population of bubbles will emerge from the test surface. All bubbles that appear must have initiated from cavities with effective radii greater than or equal to the equilibrium radius. At a given system condition the concentration is recorded and a photograph taken from which bubbles are counted. Subsequently the concentration is lowered by reducing the flow rate. When a steady concentration prevails, the old bubbles are wiped from the surface. After wiping the surface, another population soon will appear consisting of fewer bubbles and the process repeated at progressively lower concentrations until no bubbles reappear. In this way the cumulative nucleation site density, n/A vs ρ, can be obtained. If it is desired, individual sites can be singled out for study.

RESULTS AND DISCUSSION

Heat Flux Model

In order to verify the basic transient boiling model (Equation (8)), water and methyl alcohol were boiled on copper with different surface finishes. The number of active sites per in^2, n/A, was visually determined in the isolated bubble region at each q/A and ΔT. Experimental results are plotted on Figure 6. Values of f and D_b were taken from Reference [20]. The excellent agreement indicates that the process is indeed one of transient conduction and is predicted accurately by Equation (2).

It should be noted that Equation (2) not only predicted the right trend, i. e. $(q/A)_b \sim n/A$, but also the actual value of $(q/A)_b$. Some other data (e. g. [2]) indicates that $q/A \sim (n/A)^a$ where a is in general different from unity. The reason for the difference is that the

natural convection component was subtracted from the total heat flux in the present work, yielding only the boiling component. At relatively low heat fluxes, the natural convection contribution is significant.

Effective Radius of Nucleation

A polished copper test section boiled water and several organic liquids with the apparatus previously described. The heat flux was lowered to a point at which only about 8 cavities were active. Subsequently the heat flux was gradually decreased and the ΔT recorded when bubble production from each cavity ceased.

Another independent determination of ρ for the same 8 cavities was made using the gas diffusion technique described earlier. Due to experimental difficulty in maintaining a sufficiently high gas concentration for organics, only gas diffusion experiments for water were used.

Figure 8 shows a comparison of the effective radius as calculated in the boiling and gas diffusion experiments. The good agreement for water suggests that Equation (3) properly predicts the effective radius for saturated systems. In addition to verifying Equation (3) for systems whose bulk is at the saturation temperature, the good agreement shown in Figure 8 demonstrates that the gas diffusion method is a valid technique for determining the effective radius of natural cavities.

The effective radii for organics is seen to be about one half that of water. Based on the trapping model the difference between the predicted ρ for water and organics should be expected since these organics have very small contact angles compared with water; therefore ρ/R is smaller for organics on the same cavity, Figure 3.

When the ΔT for water was lowered slightly below the point at which bubble production ceased and then increased, the cavities reactivated at

the same ΔT. Similarly in the gas diffusion experiment a site which deactivated below a given concentration would again reestablish activity at the same value upon increasing concentration. Generally the organics exhibited a somewhat lesser ability than water to reactivate at a given ΔT.

A more quantitative description of the decrease in effective radius can be obtained by considering a particular cavity, say #1 (Figure 7) for which $\rho_{org}/\rho_{H_2O} \approx 1/2$. Measurements suggest that the approximate magnitude of advancing contact angles for water and organics are 35° and 7° respectively. With these contact angles and $\rho_{org}/\rho_{H_2O} = 1/2$, a cavity cone angle of $\Phi = 5°$ is obtained from Figure 3. Note also that for this cavity water has a sufficiently high contact angle to be limited by the cavity radius, i. e. $\rho/R = 1$ for water. For cavities #3, 4, 5 and 7 approximately the same Φ value of 5° is obtained. Apparently cavities #8 and 9 have Φ values greater than 7° and hence are washed out by organics. Cavity #10 has a Φ value somewhat greater than 5°, say 6°.

According to the model, the geometrical cavity radius should agree with that predicted from Equation (3) for the water data. Indeed the majority of the cavity radii as determined from photo and electron micrographs support the model as shown in Table 1. For cavities #1, 7, 9 and 10 the agreement is excellent while for cavities #3 and 5 the radii are larger than predicted from Equation (3).

TABLE 1

COMPARISON OF PHOTOGRAPHICALLY DETERMINED CAVITY RADIUS WITH EFFECTIVE RADIUS FROM BOILING AND GAS DIFFUSION EXPERIMENTS FOR WATER

Cavity #	Effective Radius x 10^4 (in)		
	Boiling	Gas Diffusion	Photograph
#1	1.05	1.12	1.0
#3	.98	1.05	1.0

Table 1 (cont.)

Cavity	Boiling	Gas Diffusion	Photograph
#5	1.15	1.35	2.7
#7	1.12	1.30	1.1
#9	1.65	1.45	1.5
#10	1.45	1.55	1.5

Typical cavity photographs and sketches are shown in Figure 9. Since the cavity shapes as sketched in Figure 8 are not ideal straight walled cones as modelled in Figure 3, the ϕ values associated with them should be regarded as effective values. The cone angles as derived from the sketches for these cavities and others, which are not shown, were approximately 30°, which is considerably larger than the 5° or 6° as deduced from the model. It is quite possible that the microscopic advancing contact angles for organics and water are much larger than 7° and 35°, respectively, or that dynamic effects also play an important role in this process. The latter effects are presently under investigation.

Active Site Density

Boiling experiments were conducted with water and several organic fluids boiled on the same surface. The cumulative site density n/A vs. ΔT was obtained by visual counting and ΔT converted to ρ from Equation (3). Figures 9 and 10 show typical results from this study and Reference [2] for different surface finishes. Notice that the n/A vs. ρ distributions are approximately straight parallel lines on log-log plots which is consistent with the surface model. Furthermore, since the organics have nearly the same contact angle, they should indeed yield similar nucleation site densities. Water has a higher contact angle and hence

lies farther to the right. The large slopes of these curves suggest a narrow band distribution of mouth radii resulting as a consequence of the very uniform surface finishing procedure that was employed.

In Reference [27] the cumulative site density versus wall superheat, n/A vs. ΔT, was obtained for several organics boiled on the same surface. In Figure 11, the data is replotted by converting ΔT to ρ from Equation (3). As expected, the data falls nearly on a single curve.

From the work of Hatton and Hall [28], who boiled water at different pressures on similar surfaces, data for n/A vs. ΔT can be obtained. Figure 12 shows some of this data replotted on n/A vs ρ coordinates using the steam tables. The data falls nearly on a single curve for each pressure as shown, revealing that Expression (3) can properly predict the pressure dependence.

It is evident from Figures 9 and 10 that the experimental results are in qualitative agreement with the prediction (Figure 4), which is based on the experimental distribution of cavity mouth radii and the model of effective radius of nucleation. The experimental data for organics and water can be interpreted quantitatively utilizing the introduced model.

Boiling Curve

Figure 13 shows the boiling curves for water, benzene and methanol. The regions where the active cavity sites are counted are denoted by "isolated bubble" regions. The following observations can be made from the results shown in the figure and the corresponding active site density curves which are not shown but are similar to those in Figures 10 and 12. The slopes of the boiling curves are determined by the slopes of the corresponding active site distributions, specifically, $(q/A)_b \sim (\Delta T)^{m+1}$

as predicted by Equation (8) where m is an exponent determined by the active site distribution, i. e. $n/A \sim R^{-m}$ or $n/A \sim \Delta T^{m}$. Furthermore it is evident from Figure 13 that, although the analysis leading to Equation (8) was based on the isolated bubble region conditions, the result of the model can be extended to the whole region of nucleate boiling. Equation (8) therefore could be used for predicting pool nucleate boiling performance of a surface, provided that the m, R_s, and Φ for the surface are known.

CONCLUSIONS

1. A transient heat conduction model can accurately describe the boiling curve for water and organics at atmospheric pressure.

2. A single cavity will have different effective radii of nucleation for different liquids. A trapping mechanism and a geometrical model relate the effective radius of nucleation to the geometry of the cavity and the contact angle.

3. A gas diffusion experiment was developed which can predict the effective radius of nucleation for natural cavities in water.

4. The cumulative site density was related to the surface properties and the contact angle. For a given surface more active sites are present at a particular effective radius for water than for organics.

5. The nucleation criteria $\Delta T = \frac{2\sigma T_s v_{fg}}{h_{fg}\rho}$ is valid for small natural cavities, even for systems whose bulk is not uniformly superheated.

REFERENCES

1. Corty, C. and A. S. Foust, "Surface Variables in Nucleate Boiling," Chem. Engg. Prog. Symp. Series, Vol. 51, No. 17, p. 1 (1955).

2. Kurihara, H. M. and J. E. Myers, "The Effects of Superheat and Surface Roughness on Boiling Coefficients," A. I. Ch. E. Journal, Vol. 6, No. 1, p. 83 (1960).

3. Mikic, B. B. and W. M. Rohsenow, "A New Correlation of Pool Boiling Data Including the Effect of Heating Surface Characteristics," J. of Heat Transfer, Vol. 91, pp. 245-250 (1969).

4. Kuhloor, N. R. and V. N. Radhakrishnan, "Effect of Surface Roughness on Nucleate Boiling," Chemical and Process Engg., pp. 276-286, June 1966.

5. Vachon, R. I., G. E. Tangler, D. L. Davis and G. H. Nix, "Pool Boiling on Polished and Chemically Etched Stainless-Steel Surfaces," J. of Heat Transfer, Vol. 90, No. 2, pp. 231-238 (1968).

6. Cooper, M. G. and A. J. P. Lloyd, "The Microlayer in Nucleate Pool Boiling," International Journal of Heat and Mass Transfer, Vol. 12, pp. 895-913 (1969).

7. Griffith, P. and J. D. Wallis, "The Role of Surface Conditions in Nucleate Boiling," Chem. Engg. Prog. Symp. Series, Vol. 56, No. 30, pp. 49-63 (1960).

8. Shai, I. and W. M. Rohsenow, "The Mechanism of Nucleate Pool Boiling Heat Transfer to Sodium and the Criteria for Stable Boiling," M. I. T. Engineering Projects Laboratory Report No. DSR 7630-45 (1967).

9. Marto, P. J. and W. M. Rohsenow, "The Effects of Surface Conditions on Nucleate Pool Boiling Heat Transfer to Sodium," M. I. T. Engineering Projects Laboratory Report No. DSR 5219-33 (1965).

10. Deane, C. W., IV, and W. M. Rohsenow, "Mechanism and Behavior of Nucleate Boiling Heat Transfer to the Alkali Liquid Metals," M. I. T. Engineering Projects Laboratory Report No. DSR 76303-65 (1969).

11. Han, C. Y. and P. Griffith, "The Mechanism of Heat Transfer in Nucleate Pool Boiling - Part I," International Journal of Heat and Mass Transfer, Vol. 8, pp. 887-904 (1965).

12. Han, C. Y. and P. Griffith, "The Mechanism of Heat Transfer in Nucleate Pool Boiling - Part II," International Journal of Heat and Mass Transfer, Vol. 8, pp. 905-914 (1965).

13. Hsu, Y. Y., "On the Size Range of Active Nucleation Cavities on a Heating Surface," J. of Heat Transfer, Vol. 84, p. 207 (1962).

14. Bergles, A. E. and W. M. Rohsenow, "The Determination of Forced Convection Surface Boiling Heat Transfer," J. of Heat Transfer, Vol. 86, Series C, No. 3 (1964).

15. Howell, J. R. and R. Siegel, "Incipience, Growth and Detachment of Boiling Bubbles in Saturated Water From Artificial Sites of Known Geometry," 3rd Intern. Heat Transfer Conf., Chicago, Vol. 4, p. 12 (1966).

16. Bankoff, S. G., "Entrapment of Gas in the Spreading of a Liquid Over a Rough Surface," A. I. Ch. E. Journal, Vol. 4, p. 24 (1958).

17. Lorenz, J. J., "The Effects of Surface Conditions on Boiling Characteristics," Ph. D. Thesis, Department of Mechanical Engineering, M. I. T., December 1971.

18. Cole, R. and W. M. Rohsenow, "Correlation of Bubble Departure Diameters for Nucleate Boiling," presented at the 10th National Heat Transfer Conf., A. I. Ch. E., August 1968.

19. Cole, R., "Bubble Frequencies and Departure Volumes at Subatmospheric Pressures," A. I. Ch. E. Journal, Vol. 13, No. 4, pp. 779-783 (1967).

20. Tolubinsky, V. I. and J. N. Ostrovsky, "On the Mechanism of Boiling Heat Transfer," International Journal of Heat and Mass Transfer, Vol. 9, p. 1463 (1966).

21. Buel, W. M. and V. W. Westwater, "Bubble Growth by Dissolution: Influence of Contact Angle," A. I. Ch. E. Journal, Vol. 12, No. 3, pp. 571-576 (1966).

22. Brown, W. T., Jr., "Study of Flow Surface Boiling," Ph. D. Thesis, Department of Mechanical Engineering, M. I. T., June 1967.

23. Hatsopoulos, G. N. and J. H. Keenan, Principles of General Thermodynamics, John Wiley and Sons (1965).

24. Johnson, M. J. and J. Borkowski, "Steam Sterilizable Probes for Dissolved Oxygen Measurement," Biotechnology and Bioengineering, Vol. 6, pp. 457-468 (1964).

25. Johnson, M. J. and J. Borkowski, "Long Lived Steam Sterilizable Membrane Probes for Dissolved Oxygen Measurement," Biotechnology and Bioengineering, Vol. 9, Issue 4, p. 635 (1967).

26. Heled, Y. and A. Orell, "Characteristics of Active Nucleation Sites in Pool Boiling," International Journal of Heat and Mass Transfer, Vol. 10, pp. 553-554 (1967).

27. Anderson, D. L. R., R. L. Judd, and H. Mette, Jr., "Site Activation Phenomena in Saturated Nucleate Boiling," A. S. M. E. Paper No. 70-HT-14 (1971).

28. Hatton, A. P. and I. S. Hall, "Photographic Study of Boiling on Prepared Surfaces," 3rd Intern. Heat Transfer Conf., Chicago, Vol. 4, p. 24 (1966).

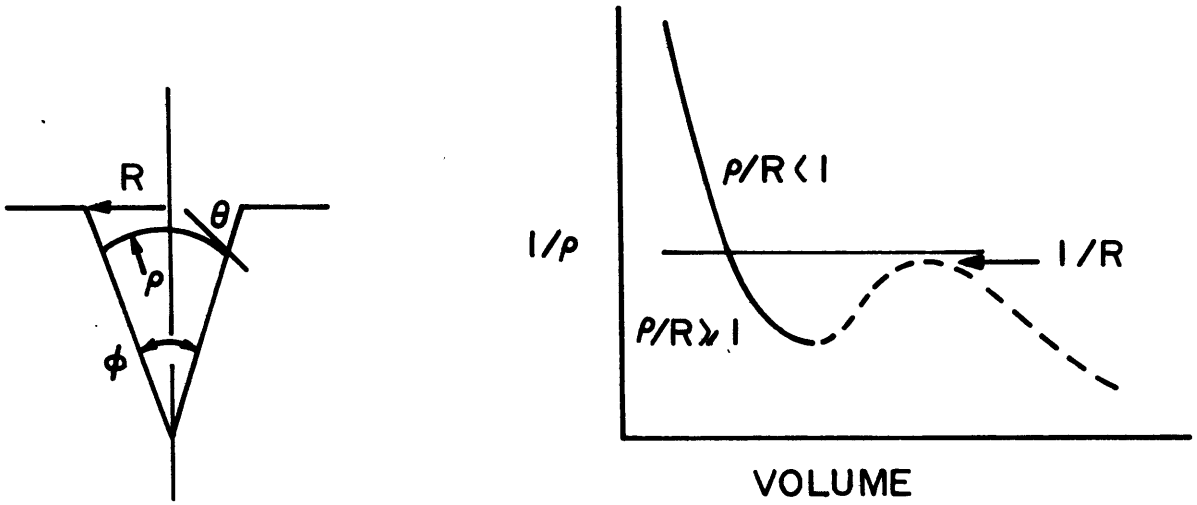

FIG 1

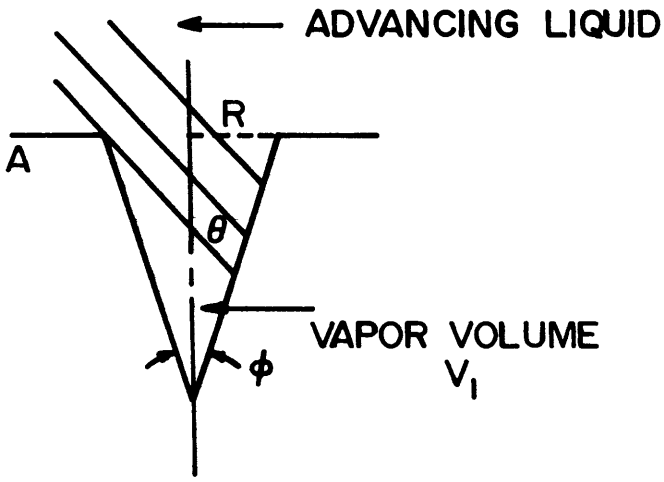

a. VAPOR TRAPPING PROCESS

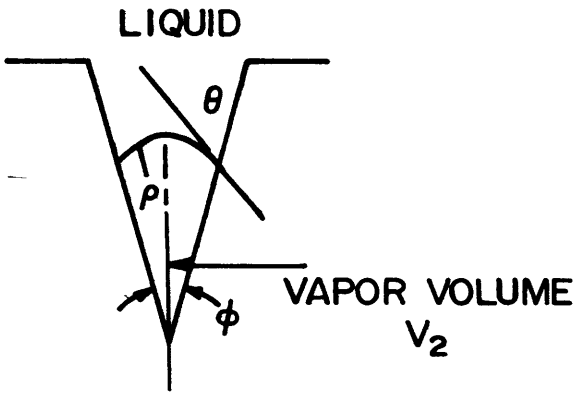

b. FORMATION OF RADIUS OF CURVATURE

FIG 2

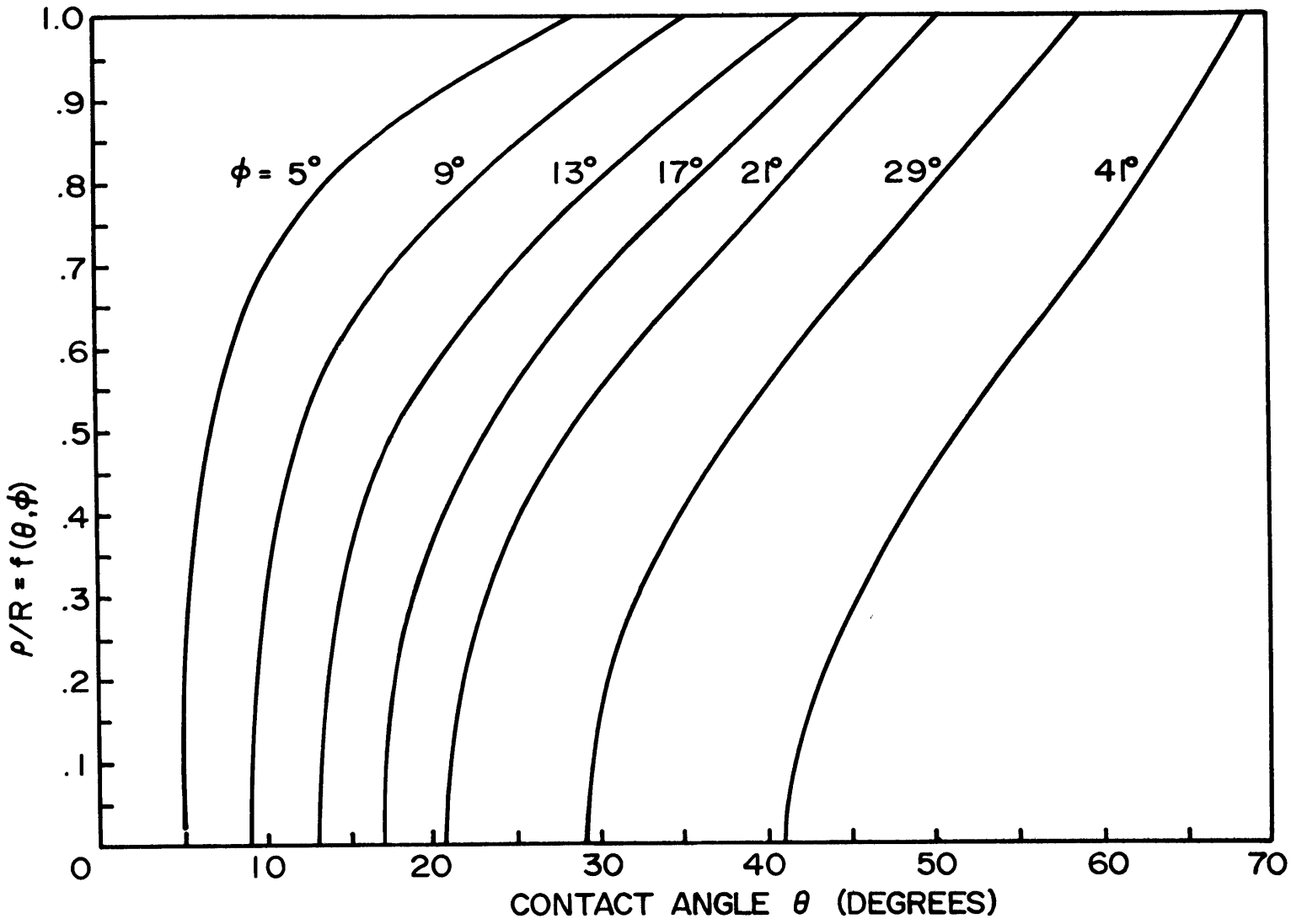
1.0
.9
.8
.7
.6
.5
.4
.3
.2
.1
0
10
20
30
40
50
60
70
ρ/R = f(θ,φ)
φ = 5°
9°
13°
17°
21°
29°
41°
CONTACT ANGLE θ (DEGREES)

Fig 3

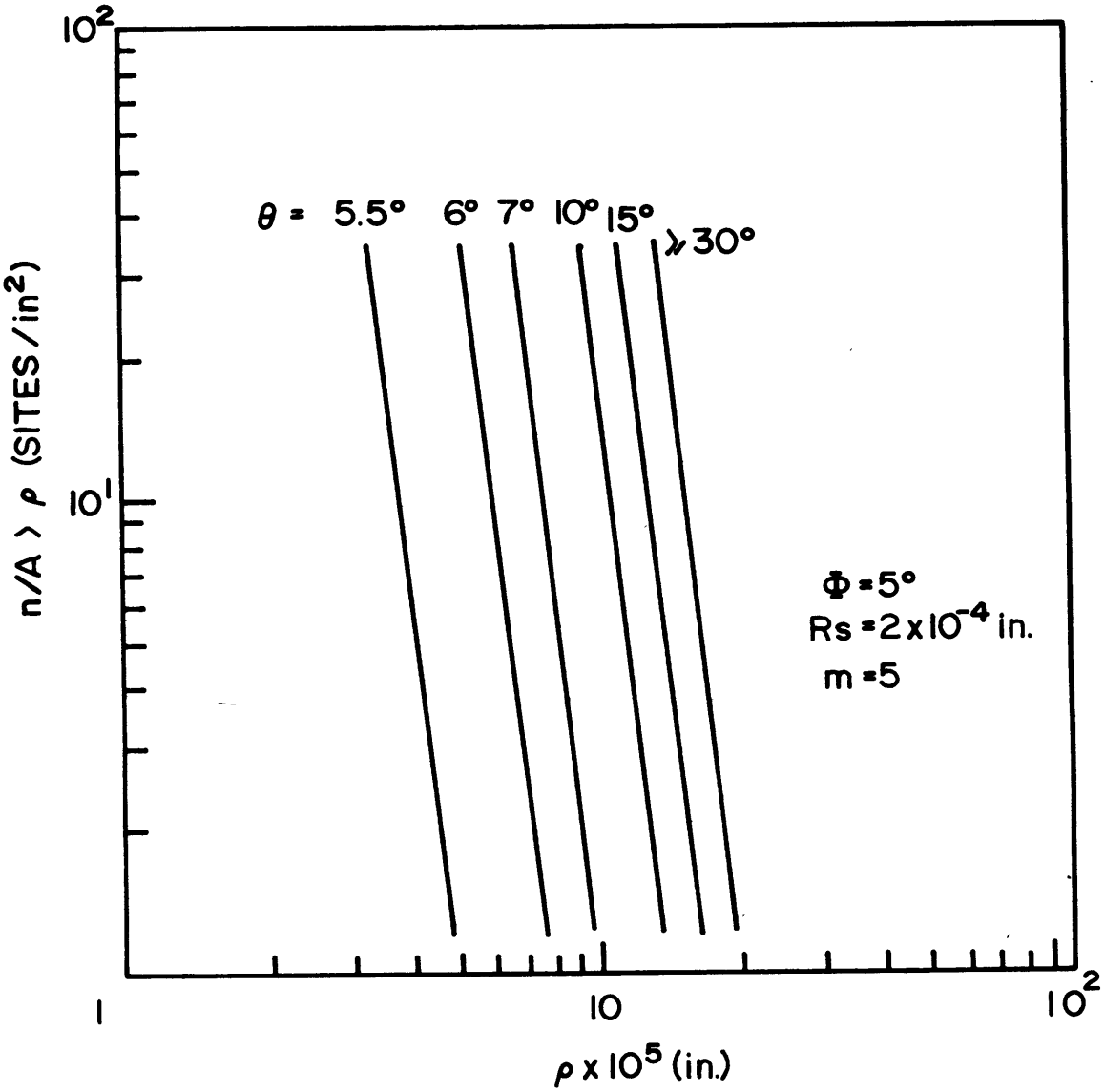
10^2
10^1
n/A > ρ (SITES/in²)
θ = 5.5° 6° 7° 10° 15° ≥30°
Φ=5°
Rs=2x10⁻⁴ in.
m=5
1
10
10^2
ρ x 10^5 (in.)

FIG 4.

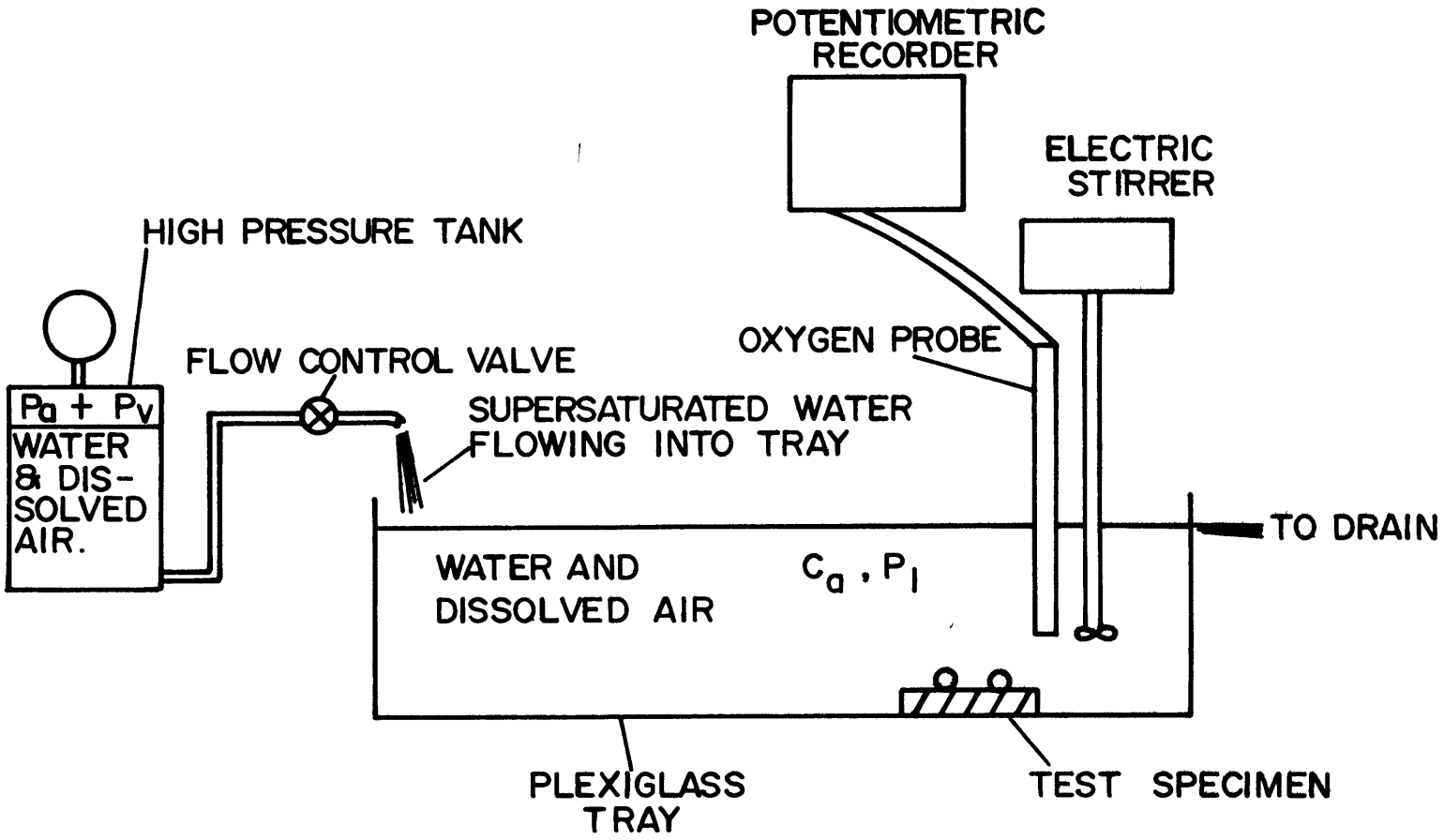
POTENTIOMETRIC
RECORDER
ELECTRIC
STIRRER
HIGH PRESSURE TANK
OXYGEN PROBE
FLOW CONTROL VALVE
Pa + Pv
WATER
& DIS-
SOLVED
AIR.
SUPERSATURATED WATER
FLOWING INTO TRAY
TO DRAIN
WATER AND
DISSOLVED AIR
Ca , P1
PLEXIGLASS
TRAY
TEST SPECIMEN

FIG 5

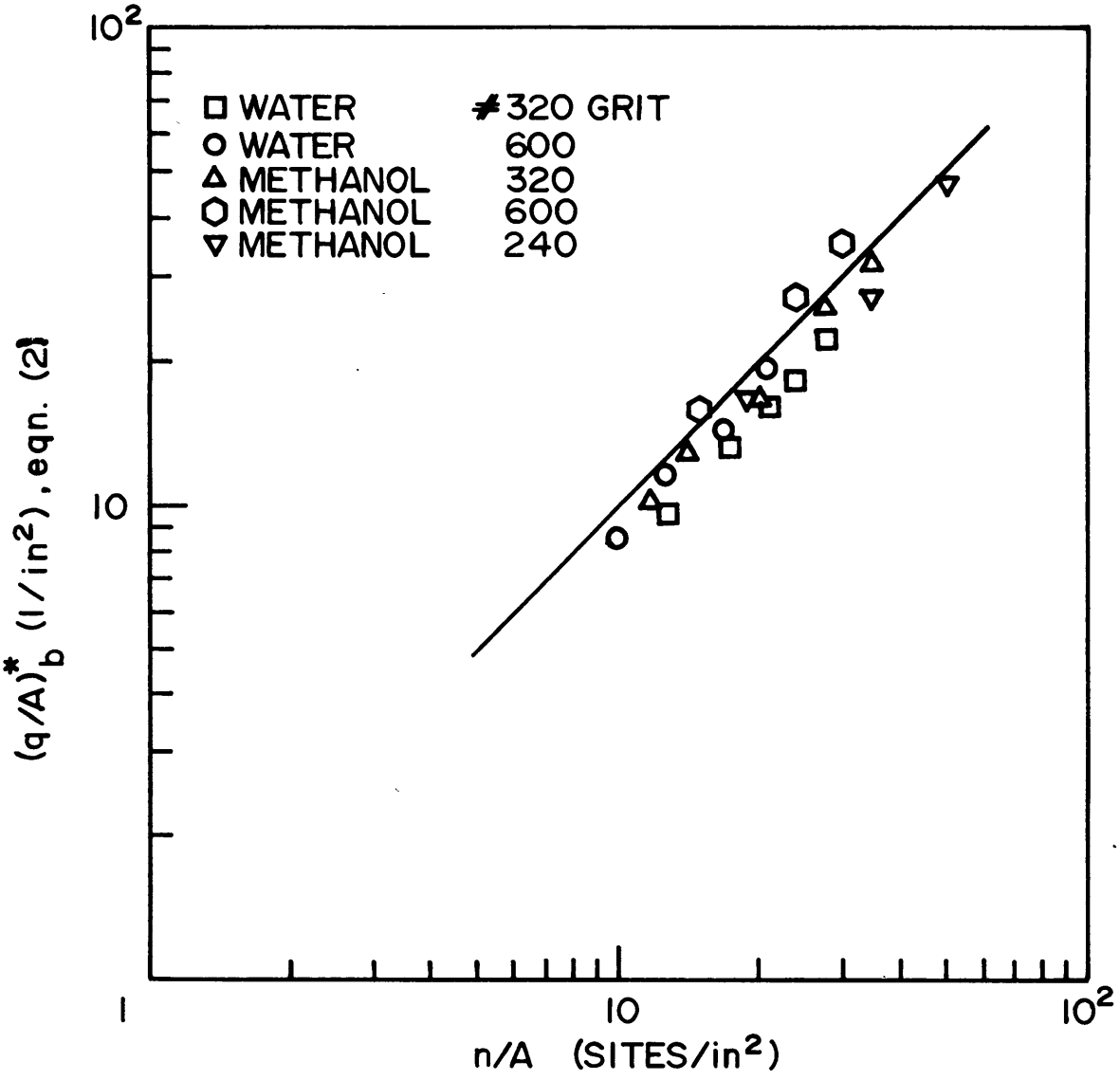
10²
10
1
10
10²
□ WATER #320 GRIT
○ WATER 600
△ METHANOL 320
⬡ METHANOL 600
▽ METHANOL 240
(q/A)*b (1/in²), eqn. (2)
n/A (SITES/in²)

FIG 6

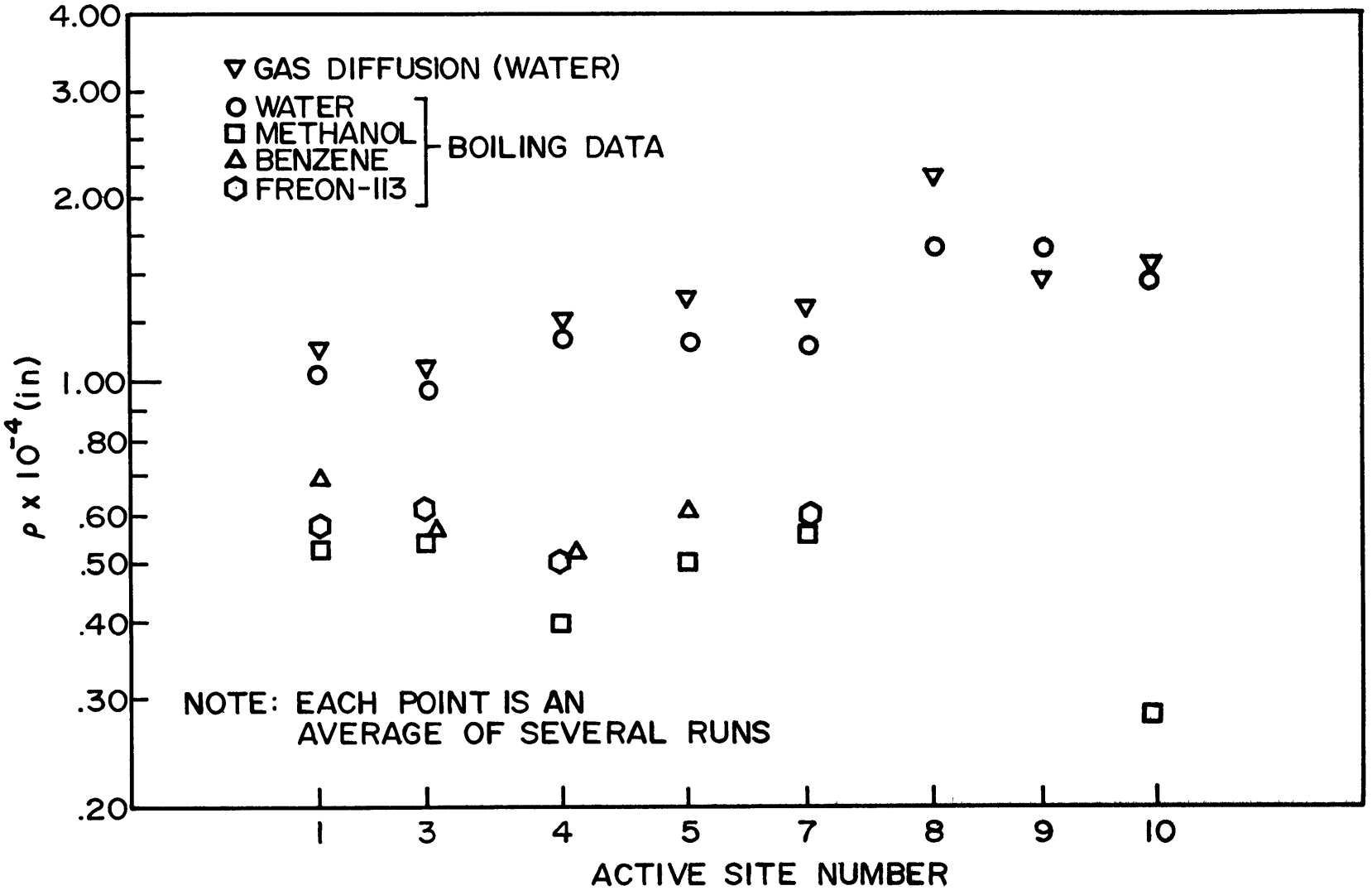
4.00
3.00
2.00
1.00
.80
.60
.50
.40
.30
.20
ρ x 10⁻⁴ (in)
▽ GAS DIFFUSION (WATER)
○ WATER
□ METHANOL
△ BENZENE
⬡ FREON-113
BOILING DATA
NOTE: EACH POINT IS AN AVERAGE OF SEVERAL RUNS
1
3
4
5
7
8
9
10
ACTIVE SITE NUMBER

FIG 7

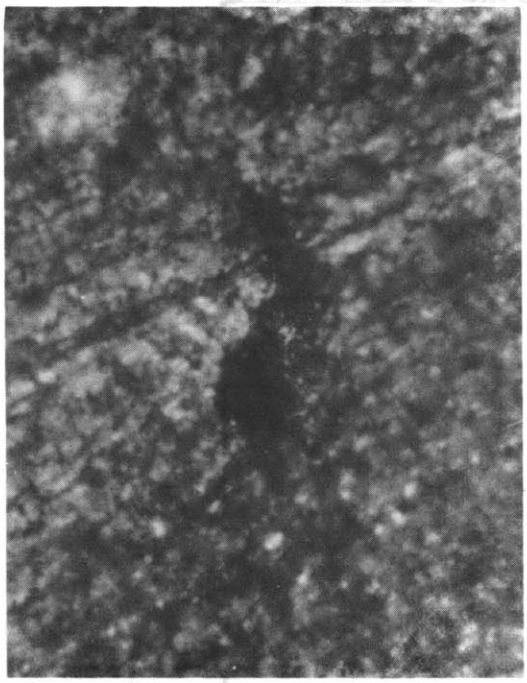

1190 x mag.

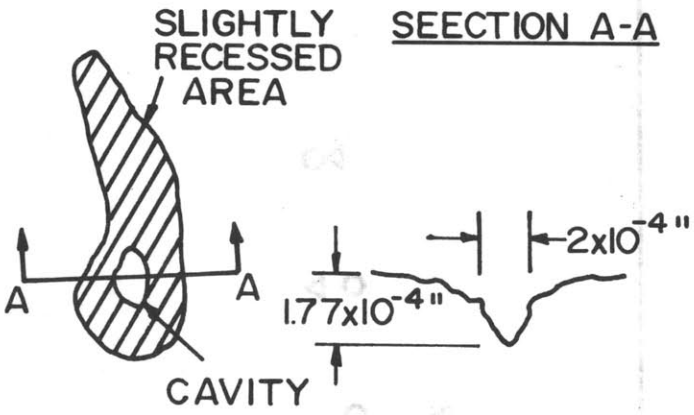

a. CAVITY # 1

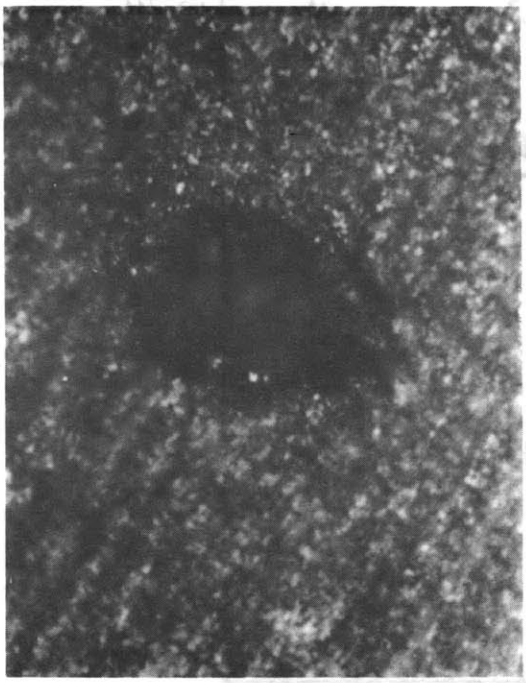

1190 x mag.

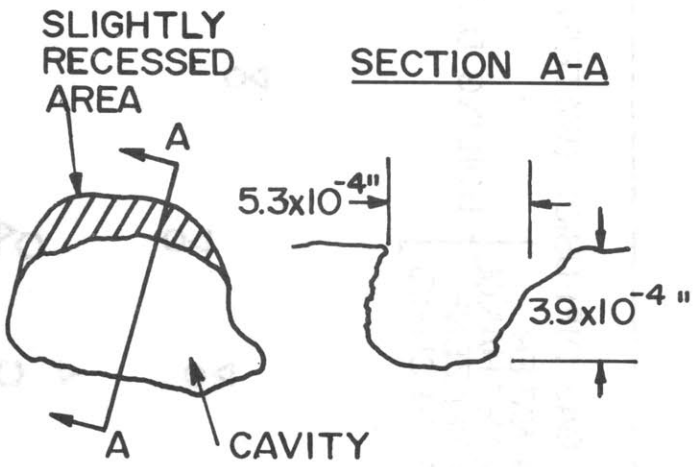

b. CAVITY # 3

FIG 8

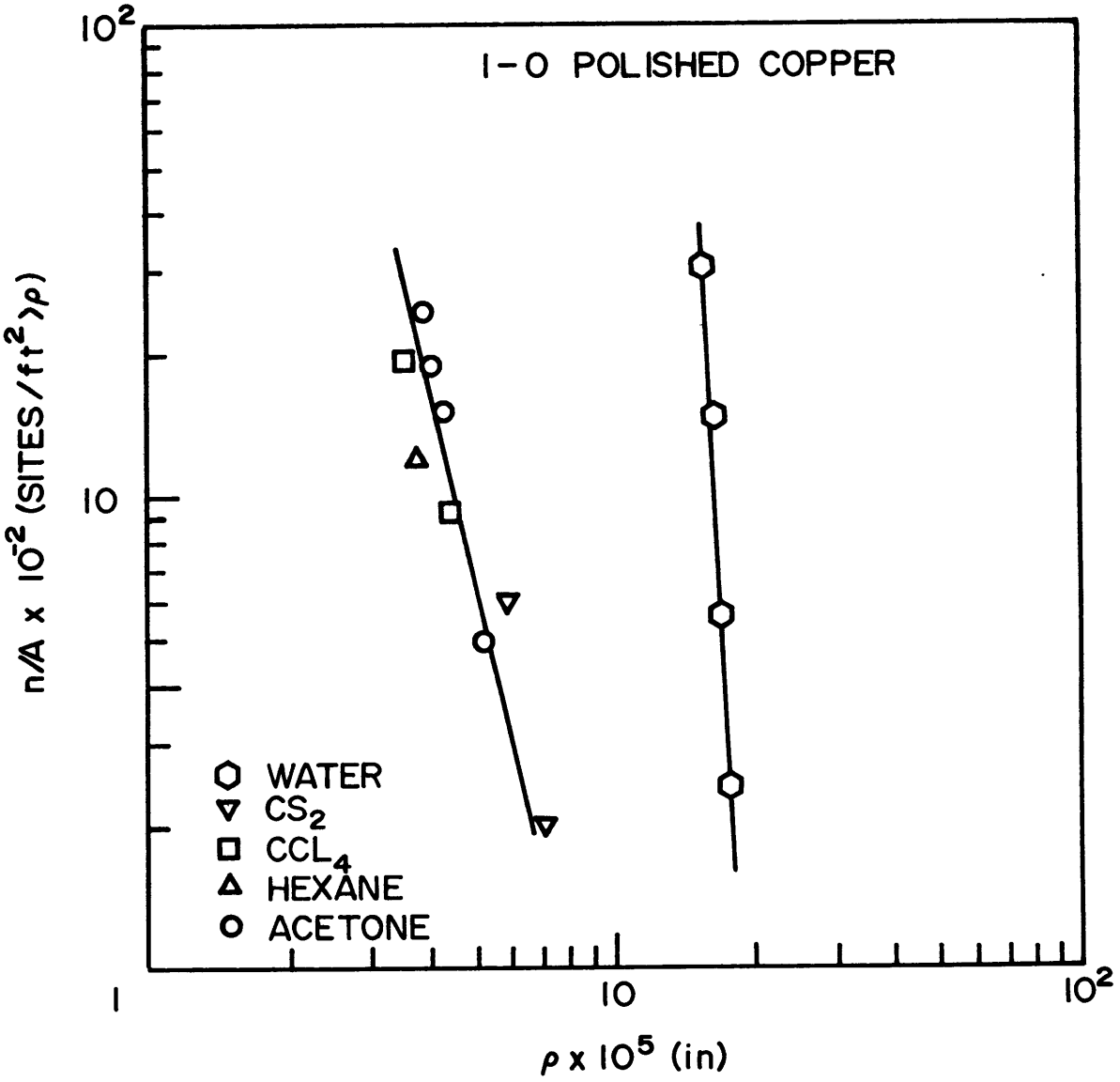
1-0 POLISHED COPPER
10^2
10
1
$n/A \times 10^{-2}$ (SITES/ft^2)
$\rho \times 10^5$ (in)
WATER
CS_2
CCL_4
HEXANE
ACETONE

FIG 9

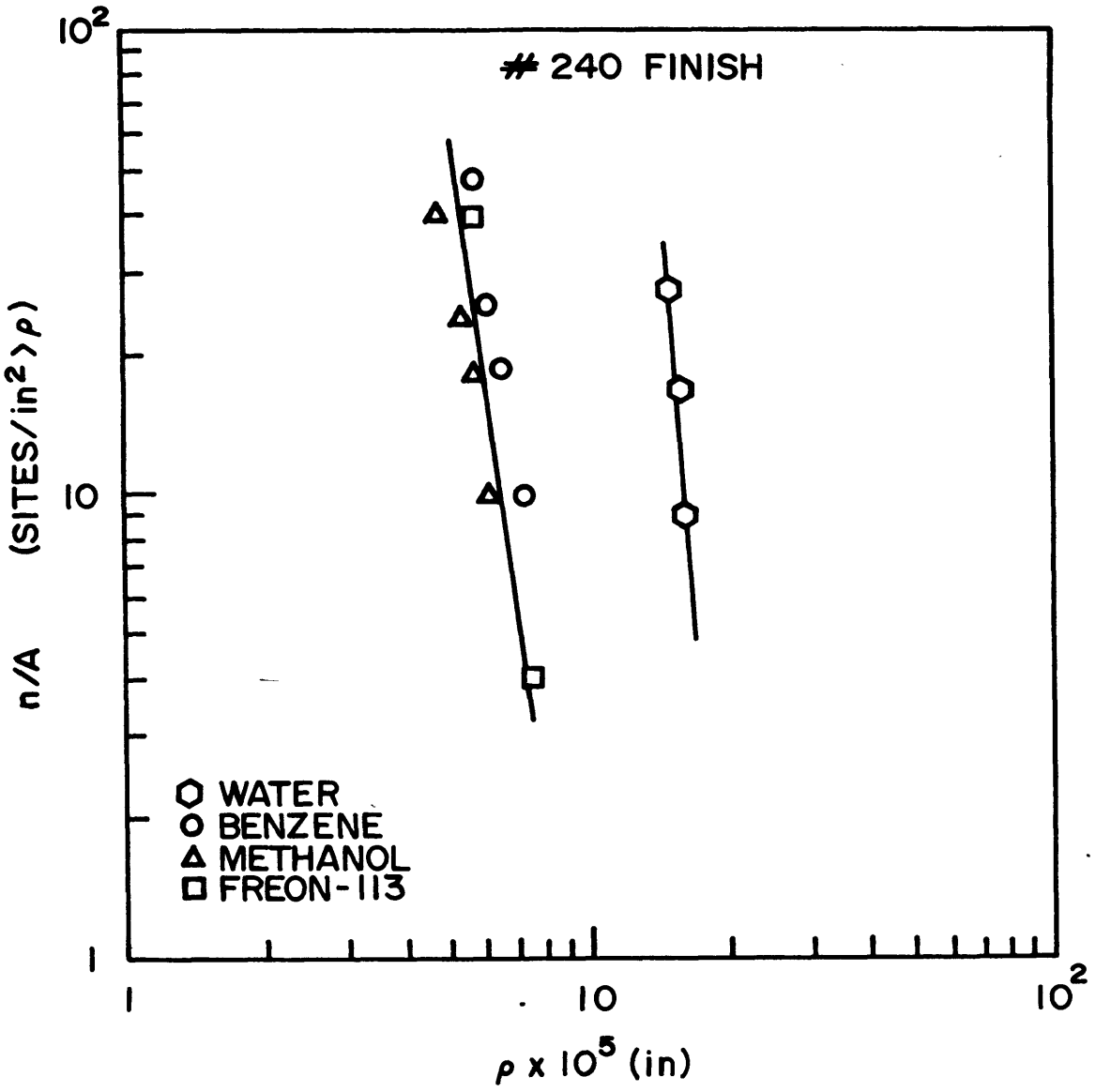
#240 FINISH
n/A (SITES/in²>ρ)
10²
10
1
1
10
10²
ρ x 10⁵ (in)
WATER
BENZENE
METHANOL
FREON-113

FIG 10

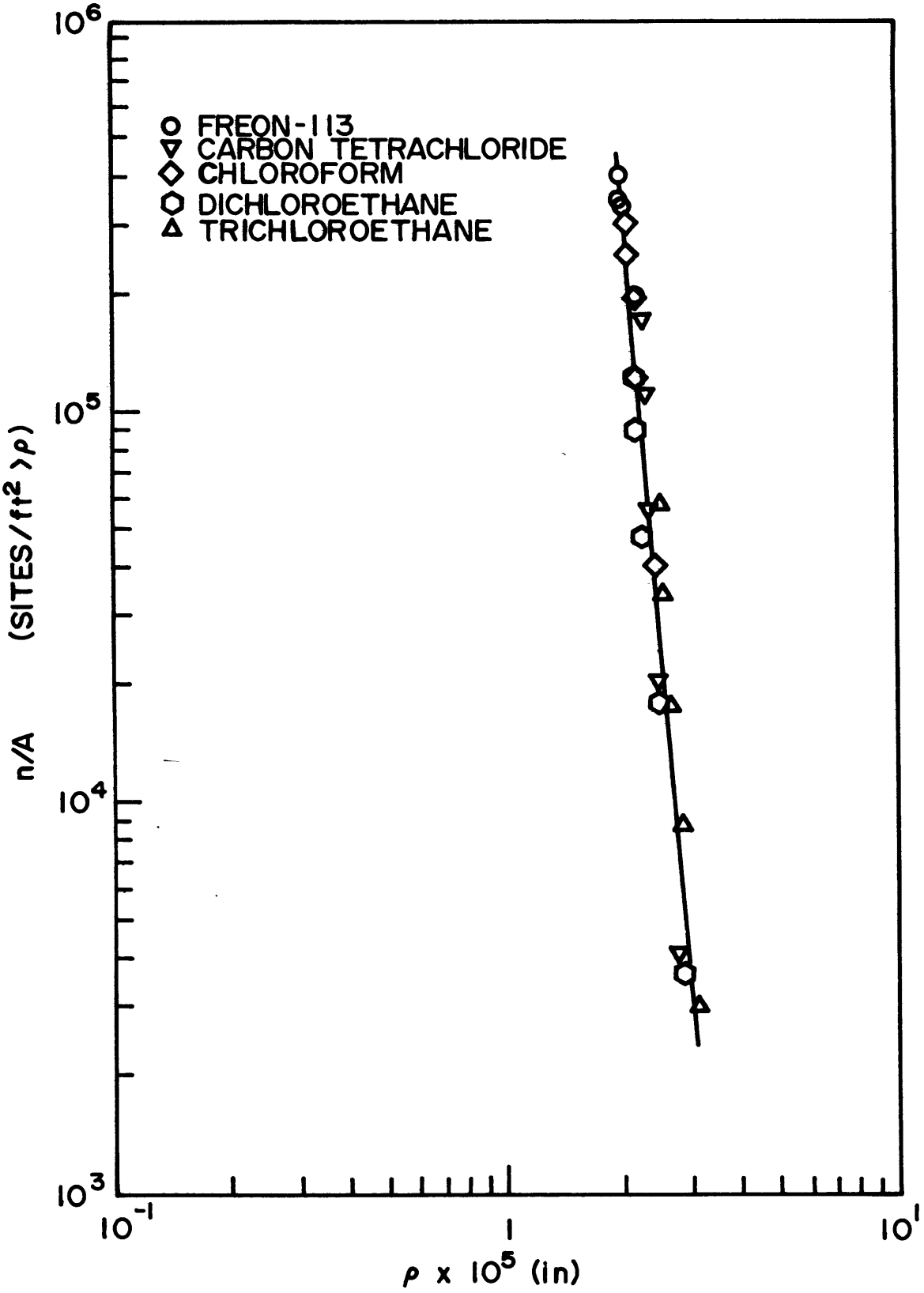
FREON-113
CARBON TETRACHLORIDE
CHLOROFORM
DICHLOROETHANE
TRICHLOROETHANE
n/A (SITES/ft² > ρ)
10⁶
10⁵
10⁴
10³
10⁻¹
1
10¹
ρ x 10⁵ (in)

FIG 11

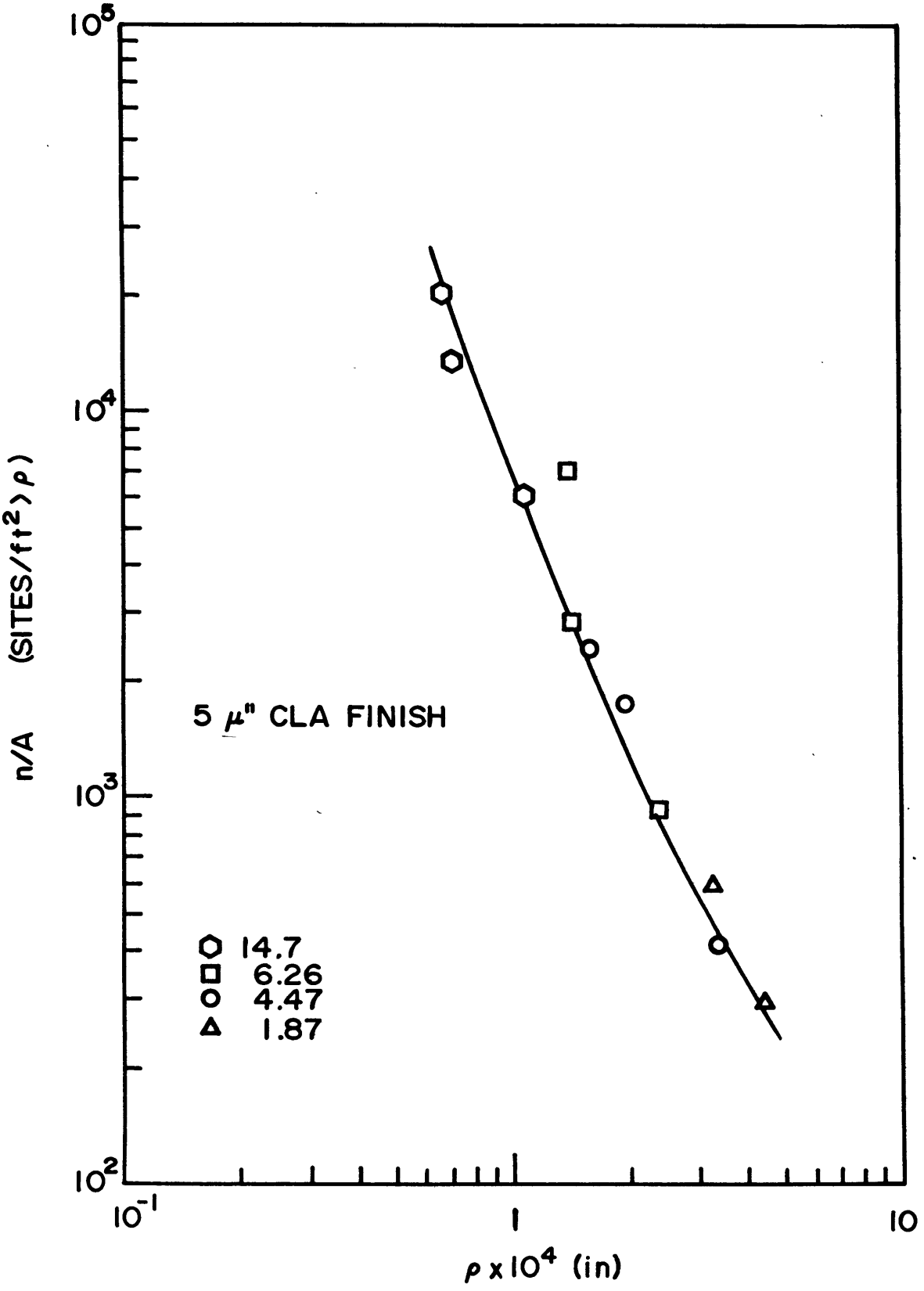
10^5
10^4
10^3
10^2
n/A (SITES/ft²)ρ)
5 μ" CLA FINISH
14.7
6.26
4.47
1.87
10^{-1}
1
10
ρ x 10^4 (in)

FIG 12

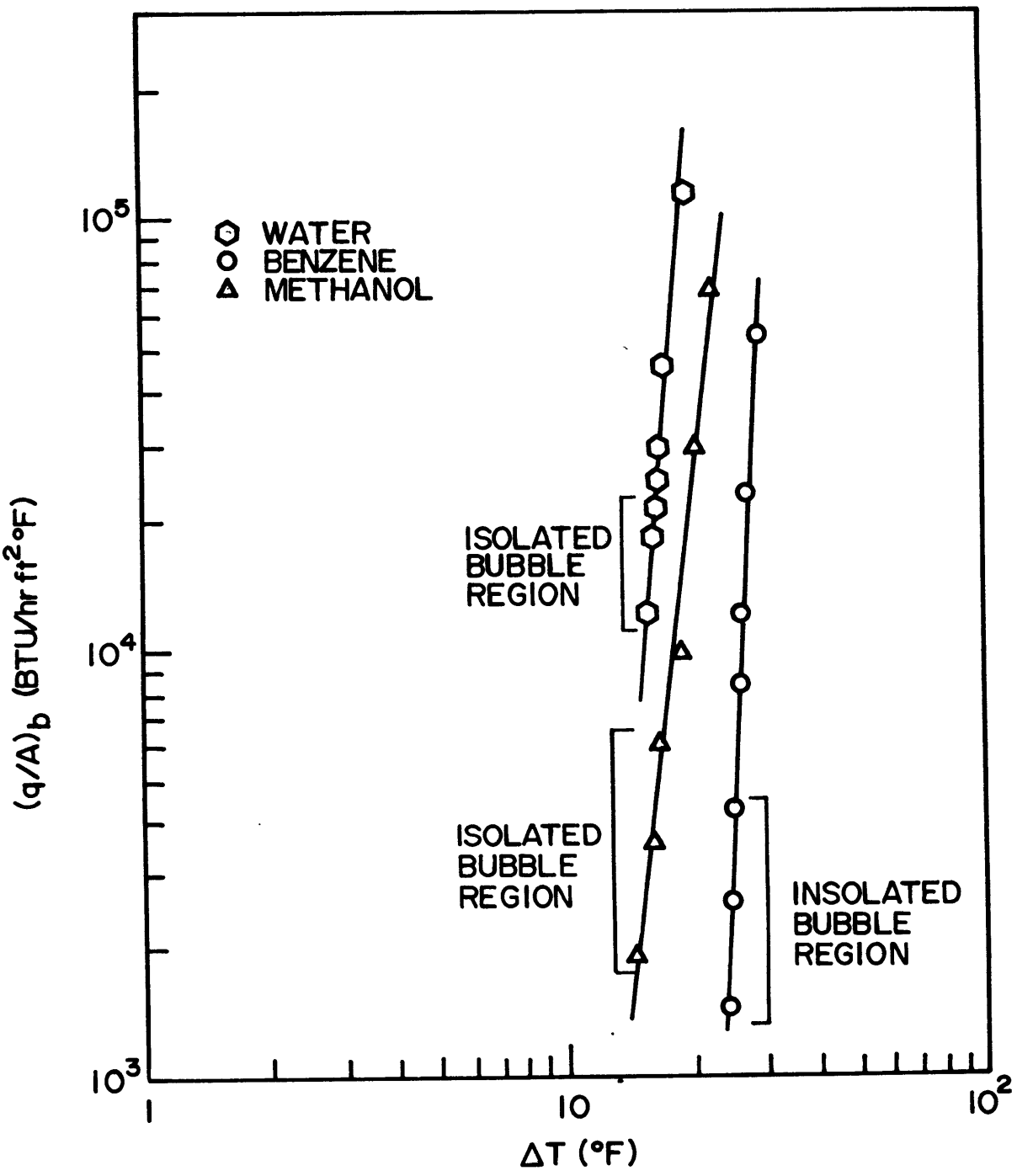
WATER
BENZENE
METHANOL
ISOLATED BUBBLE REGION
ISOLATED BUBBLE REGION
INSOLATED BUBBLE REGION
10^5
10^4
10^3
1
10
10^2
$(q/A)_b$ (BTU/hr ft^2°F)
ΔT (°F)

Fig 13